Taran, M. N., Ohashi, H., Koch-Müller, M. (2008): Optical spectroscopic study of synthetic NaScSi2O6-CaNiSi2O6 pyroxenes at normal and high pressures. - Physics and Chemistry of Minerals, 35, 3, 117-127

DOI: 10.1007/s00269-007-0202-6.

Optical spectroscopic study of synthetic $NaScSi_2O_6$ – $CaNiSi_2O_6$ pyroxenes at normal and high pressures

Michail N.Taran[1], Haruo Ohashi[2], Monika Koch-Müller[3]

[1]Institute of Geochemistry, Mineralogy and Ore Formation, National Academy of Sciences of Ukraine, Palladin Ave. 34, 03680 Kyiv-142, Ukraine

Tel: +0038 044 424-0043

taran@igmr.relc.com

[2] HASHI Institute for Silicate Science, Nishinakanobu 1-9-25, Shinagawa, Tokyo 142-0054, Japan
Tel: +81 03 3783 1798
haruohashi@hotmail.com

[3]GeoForschungsZentrum, Sektion 4.1, Telegrafenberg, 14473 Potsdam, Germany
Tel: +49(0)331-288-1492
mkoch@gfz-potsdam.de

Abstract

Six synthetic $NaScSi_2O_6$ – $CaNiSi_2O_6$ pyroxenes were studied by optical absorption spectroscopy. Five of them of intermediate $(Na_{1-x}, Ca_x)(Sc_{1-x}, Ni_x)Si_2O_6$ compositions show spectra typical of Ni^{2+} in octahedral coordination, more precise Ni^{2+} at the M1 site of the pyroxene structure. The common feature of all spectra is three broad absorption bands with maxima around 8000 cm^{-1}, 13000 cm^{-1} and 24000 cm^{-1} assigned to ${}^3A_{2g} \rightarrow {}^3T_{2g}$, ${}^3A_{2g} \rightarrow {}^3T_{1g}$ and $\rightarrow {}^3T_{1g}({}^3P)$ electronic spin-allowed transitions of ${}^{VI}Ni^{2+}$. A weak narrow peak at ~14400 cm^{-1} is assigned to the spin-forbidden ${}^3A_{2g} \rightarrow {}^1T_{2g}$ $({}^1D)$ transition of Ni^{2+}. Under pressure the spin-allowed bands shift to higher energies and change in intensity. The octahedral compression modulus, $k^{loc}_{Ni(M1)}$, calculated from the shift of the ${}^3A_{2g} \rightarrow {}^3T_{2g}$ band in the $(Na_{0.7}Ca_{0.3})(Sc_{0.7}Ni_{0.3})Si_2O_6$ pyroxene is evaluated as 85±20 GPa. The Racah parameter B of Ni^{2+}(M1) is found gradually changing from ~919 cm^{-1} at ambient pressure to ~890 cm^{-1} at 6.18 GPa.

The Ni end-member pyroxene ($(Ca_{0.93}\ Ni_{0.07})NiSi_2O_6$) has a spectrum different from all others. In addition to the above mentioned bands of Ni^{2+}(M1) it displays several new relatively intense and broad extra bands which were attributed to electronic transitions of Ni^{2+} at the M2 site. In difference to CaO_8 polyhedron geometry of an eight-fold coordination, $Ni^{2+}(M2)O_8$ polyhedra are assumed to be relatively large distorted octahedra. Due to different distortions and different compressibilities of the M1 and M2 sites the Ni^{2+}(M1)- and Ni^{2+}(M2)-bands display rather different pressure-induced behaviors, becoming more resolved in the high-pressure spectra than in that measured at atmospheric pressure. The octahedral compression modulus of Ni^{2+}(M1) in this end-member pyroxene is evaluated as 150±25 GPa, which is noticeably larger than in $Ni_{0.3}$ pyroxene. This is due to a smaller size and, thus, a stiffer character of $Ni^{2+}(M1)O_6$ octahedron in the $(Ca_{0.93}\ Ni_{0.07})NiSi_2O_6$ pyroxene compared to $(Na_{0.7}Ca_{0.3})(Sc_{0.7}Ni_{0.3})Si_2O_6$.

Key words: optical absorption spectra; Ni^{2+}; pyroxene; high-pressure

Introduction

Crystal field spectra of Ni^{2+} in natural and synthetic crystals are poorly studied in comparison with other transition metal ions, especially Fe^{2+} and Cr^{3+}. Predominantly, these studies are based on powder reflectance spectra: just a few publications can be found in literature on Ni^{2+}-single crystal spectroscopy (Rossman et al. 1981; Hu et al. 1990; Solntsev et al. 2006). And, as far as we know, no one investigated high-pressure spectra of Ni^{2+}-containing crystals.

It is remarkable that Ni^{2+} has d^8 electronic configuration and, according to the crystal field theory (e.g. Sviridov et al. 1976, Marfunin 1979, Burns 1993), it acquires – similar to $^{VI}Cr^{3+}$ – the highest crystal field stabilization energy (CFSE). However, some authors also suggest that Ni^{2+} enters tetrahedral structural sites (e.g. Tejedor-Tejedor et al. 1983, Solntsev et al. 2006). The high CFSE of $^{VI}Ni^{2+}$ may play an important role in such phenomena as isomorphism, inter- and intracrystalline cation distribution or distribution of Ni^{2+} between crystal phases and melt and, for example may cause a different distribution of Ni^{2+} among the two non-equivalent octahedral sites M1 and M2 in the pyroxene structure. In olivine, for instance, where the cationic M1 and M2 sites do not differ by dimension and symmetry as much as in pyroxene, Ni^{2+} enters both sites with a large preference for the smaller M1 (Boström 1987, Ottonello et al. 1989). Note that in olivine Ni^{2+} causes prominent optical absorption spectra (e.g. Hu et al. 1990; Langer 2000) which behavior under thermal treatment were used to investigate the equilibrium and kinetics of the Ni-Mg-distribution, for instance (Garsche and Langer 1994). In this junction it is interesting to elucidate whether Ni^{2+}, like Cr^{3+}, prefers the smaller M1 rather than the larger M2 site of the pyroxene structure. Besides, it would be interesting to compare the pressure behavior of Ni^{2+}-bearing pyroxene and calculated from it the polyhedral compressibilities and the character of the Ni-O bond with those of Cr^{3+}-bearing minerals. Synthetic $NaScSi_2O_6$-$CaNiSi_2O_6$ pyroxenes crystallized as small but well formed transparent crystals appropriate for microspectroscopic studies are a good object for such investigation. To study the Ni^{2+}-

distribution over the two sites, M1 and M2 and the pressure behavior of the corresponding crystal field spectra we investigated synthetic Ni-bearing pyroxenes by optical spectroscopy.

Details of experiments

Pyroxenes of six different compositions were synthesized by solid state reaction using a belt type high-pressure apparatus (Fukunaga et al. 1979) at 6 GPa and 1500 °C (Ohashi et al. 1997). They were recrystallized from clinopyroxene powders grown at atmospheric pressure. The latter were obtained by solid state reaction using a SiC resistance furnace and Na_2CO_3, $CaCO_3$, Sc_2O_3, NiO, SiO_2 as starting materials (Ohashi 1988). Their stoichiometric mixtures were sintered in Pt crucibles and heated at 1 atm to 1100-1300 °C.

The clinopyroxenes studied here were available as small (ca. 30×80 μm) transparent crystals of elongated prismatic habit with well developed faces (Ohashi 1988; Ohashi et al. 1997). In accordance with *x* of the intended $(Na_{1-x}, Ca_x)(Sc_{1-x}, Ni_x)Si_2O_6$ composition they are labeled as $Ni_{0.1}$, $Ni_{0.2}$, $Ni_{0.3,}$ $Ni_{0.6}$, $Ni_{0.8}$ and $Ni_{1.0}$ pyroxene. It is noteworthy that the pyroxenes grown at atmospheric pressure and at 6 GPa differ by cell parameters (Ohashi et al. 1997) thus reflecting, as assumed, the differences in the electronic structure of Ni^{2+} at synthesis conditions (Ohashi 1988; Ohashi et al. 1997). Depending on the nickel content the color of the pyroxene crystals varies from light green, nearly colorless, to light greenish-yellow.

Chemical analyses of five pyroxenes, $Ni_{0.1}$, $Ni_{0.2}$, $Ni_{0.3,}$ $Ni_{0.6}$ and $Ni_{1.0}$, were determined with a Cameca SX100 electron microprobe using albite (Na), $ScPO_4$ (Sc), diopside (Si), NiO (Ni) and diopside (Ca) as standards. The microprobe analyses of the samples, each averaged over five measurements in different points along the crystal elongation, are compiled in Table 1.

Six transparent crystals of different compositions with minimum of cracks, inclusions or other visible imperfections were selected under a binocular microscope for optical spectroscopic

studies. To diminish light scattering on the lower surface, the samples were half-embedded into a droplet of glycerol upon the supporting silica glass plate.

In spite of the visually high quality, between crossed Nicols all of them display a very vague extinction in orientations not coinciding with the crystal elongation, i.e. typical for monoclinic C2/c clinopyroxenes (e.g. Tröger 1968). This observation is consistent with results of structure refinements of the end members $CaNiSi_2O_6$ and $NaScSi_2O_6$ by Ghose et al. (1987) and Ohashi et al. (1994), respectively, showing that both belong to *C2/c* clinopyroxenes. Unpolarized spectra on the raw, unpolished crystals were measured in the range 330-1000 nm (ca. 30300-10000 cm^{-1}). Spectra of three larger samples, $Ni_{0.3}$, $Ni_{0.6}$ and $Ni_{1.0}$, were measured in the broader range, 30300-4000 cm^{-1}.

Two crystals, $Ni_{0.3}$ and $Ni_{1.0}$, were prepared as platelets parallel the crystal elongation, polished on both sides. Between crossed Nicol prisms they again display a rather vague extinction. Examination at a large magnification evidences that the crystal of $Ni_{0.3}$ composition consists partly of polysynthetic twins and that of $Ni_{1.0}$ composition has apparently a micro-block structure. Because of such imperfections the conoscopic figures of both platelets are diffuse and indefinable. A weak pleochroism from pale green to yellowish-green is seen in polarized light. On these two polished platelets the polarized spectra were measured in the range 330-1800 nm (~30300-5555 cm^{-1}).

A home-made single-beam microspectrophotometer constructed on basis of a SpectraPro-275 triple grating monochromator, a highly modified polarizing mineralogical microscope MIN-8 and a PC was used for spectroscopic measurements. Ultrafluars 10× served as objective and condenser. Two photoelectric multiplying tubes and a PbS-cell, cooled by the Peltier effect to –20 °C, were used as changeable photodetectors. A mechanical high-stabilized 300 Hz-chopper and lock-in amplifier were applied to improve the signal/noise ratio. Two high-stabilized lamps, a xenon lamp and a quartz-halogen lamp, both of 70 W, were used as light sources for the ranges 330-450 nm and 450-2000 nm, respectively. The spectra were scanned with steps $\Delta\lambda$=1 nm, 2

nm and 10 nm in the range 330-450, 450-1000 and 1000-2000 nm, respectively, by means of digital wavelength-step-scanning procedure with an Acton Research Corporation SpectaCard readout system driven by Windows SC-1 control and data acquisition software. Measuring of the spectra is accomplished by a routine single-beam procedure. In all cases the diameter of the measuring spot was not larger than 15 μm.

NIR spectra in the range 11000-4000 cm^{-1} were recorded on a Bruker ISF 66v FTIR spectrometer. The spectrometer was equipped with a tungsten light source, a NIR/Quartz beam-splitter and a Hyperion microscope using Cassegrainian objectives and an InSb detector. The spectra were taken with an aperture size of 20×20 μm and a resolution of 2 cm^{-1}. For each spot the spectrum was averaged over 256 scans.

Unpolarized high-pressure spectra of two pyroxenes, a polished plate of $Ni_{0.3}$ and a rough crystal of $Ni_{1.0}$, both of ca. 30 μm thick, were measured in the range 330-1000 nm (ca. 30300-6000 cm^{-1}). For this the diamond anvil cell technique were used as described elsewhere (*e.g.* Langer et al. 1997). The gaskets were machined from hardened steel, 300 μm thick with a 300 μm diameter bore. A 4:1 mixture of methanol/ethanol served as pressure-transmitting medium. The ruby fluorescence method was used for pressure calibration. The estimated precision of the pressure determination is ±0.18 GPa.

The spectra were subject to a curve fitting process using the program Peakfit 4.11 (Jandel Scientific) and assuming a Gaussian shape for the component absorption bands.

Results and discussion

Microprobe analyses of the pyroxenes evidence that on the whole their compositions are very close to the intended ones (Tab. 1). Only one feature should be noticed: the Ni-content in the end-member pyroxene $Ni_{1.0}$ is apparently surplus, clearly evidencing that about 0.067 apfu. of Ni enters the M2 position of the pyroxene structure. The understated amount of Ca, 0.922 apfu.,

fits this observation. On this account the crystal chemical composition of this end-member $Ni_{1.0}$ pyroxene should be written as $(Ca_{0.93}\ Ni_{0.07})NiSi_2O_6$ and one may expect that the optical absorption spectrum of this pyroxene is to be qualitatively different from the others.

Indeed, we obtained two types of optical absorption spectra from the samples studied. Spectra of all pyroxenes except the end-member $Ni_{1.0}$ are assigned to type I. They are very similar among themselves differing in intensity of the observed absorption bands and in their slight shifts to higher energies with increasing Ni-content. The end-member $Ni_{1.0}$ spectrum represents the type II spectrum. It apparently differs from the others by the presence of some extra bands which are complementary to the bands observed in the type I spectra.

As an example, unpolarized spectra of three samples, $Ni_{0.3}$, $Ni_{0.6}$ (both of the type I) and $Ni_{1.0}$ (type II), are shown in Figure 1. As seen from the Figure, the common spectroscopic features in spectra of the two types are three broad absorption bands with maxima around 8000 cm^{-1}, 13000 cm^{-1} and 24000 cm^{-1}. Note that the band at 13000 cm^{-1} is complicated by a weak narrow feature at 14700 cm^{-1}. The type II spectrum is characterized by two additional extra bands around 5650 cm^{-1} and 19600 cm^{-1} which appear together with the three above mentioned bands in the type I spectrum. It should be emphasized that the two extra bands occur only in the spectrum of the end member $Ni_{1.0}$ pyroxene. There are no manifestations of them in spectra of all other samples including $Ni_{0.8}$ pyroxene, the closest by composition to $Ni_{1.0}$.

All characteristic bands in the spectra of both types are better seen in polarized spectra measured on polished plates. However, it is very difficult to prepare such oriented crystal plates because of the tiny dimensions of the pyroxene crystals and even more because of the very vague extinction between crossed Nicol prisms. With the diffuse and uncertain conoscopic figures which we observed, we were unable to orient the crystals precisely enough for preparing oriented samples and measuring polarized spectra in the three polarizations **E**||**X**, **E**||**Y** and **E**||**Z**, as it was done for natural Cr- or Fe-bearing clinopyroxenes by e.g. Taran et al. (1994) or Taran and Langer (2001). In the present case the actual orientations were accomplished by extinction

between crossed Nicols on sections randomly cut out along the elongation of the crystals. As an example, the polarized type I spectrum of $Ni_{0.3}$ pyroxene is shown in Fig. 2a. It contains five bands *a* to *e*, typical of Ni^{2+} in octahedral coordination (e.g. Sviridov et al. 1976, Marfunin 1979, Burns 1993), the three most intense bands are distinct in spectra of rough unpolished crystals in Fig. 1. These latter bands, *a*-band at ~7800 cm^{-1}, *b*-band at ~12800 cm^{-1} and *e*-band at ~23700 cm^{-1}, are to be attributed to the electronic spin-allowed *dd*-transitions $^3A_{2g} \rightarrow {}^3T_{2g}$, $^3A_{2g} \rightarrow {}^3T_{1g}$ and $^3A_{2g} \rightarrow {}^3T_{1g}(^3P)$ of $^{VI}Ni^{2+}$, respectively. A sharp, relatively weak *c*-band should be assigned to the spin-forbidden transition $^3A_{2g} \rightarrow {}^1E_g$ of $^{VI}Ni^{2+}$.[1] A vague weak shoulder around 21000 cm^{-1}, labeled as *d*, is, very likely, another spin-forbidden triplet-singlet transition, $^3A_{2g} \rightarrow {}^1T_{2g}$ (^1D).

As seen from Figure 2a, the differences between the two polarizations are mostly due to different intensities of the absorption bands, not their energies. Especially this is the case for the *a*-and *b*-bands, whereas the third spin-allowed band, *e*, displays just a slight difference in energy of about 200 cm^{-1}. This circumstance evidences that the respective excited electronic states of Ni^{2+}, $^3T_{2g}$, $^3T_{1g}$ and $^3T_{1g}(^3P)$, are nearly unsplit and, therefore, the relevant octahedral site should be relatively weakly distorted (cf. e.g. Rossman et al. 1981). This assumption is supported also by a simple shape of the *b*-band, which in many Ni^{2+}-bearing minerals and compounds is split into at least two components (Sviridov et al. 1976). In diffuse reflectance spectra of Ni-bearing phyllosilicates, for instance, such splitting is attributed to the low symmetry of the coordination octahedron of Ni^{2+} (e.g. Manceau et al. 1985, Manceau and Calas 1987). However, in the type I spectra of our pyroxenes this band is seen as a singular band slightly overlapped by the much weaker spin-forbidden band *c*. This observation is supported by results of the curve resolution of the $Ni_{0.3}$ pyroxene spectrum showing that all three spin-allowed bands *a*, *b* and *e*, as well as the two spin-forbidden ones, *c* and *d*, can be satisfactory approximated by singular Gaussians (Fig. 2b).

[1] Rossman et al. (1981) found this bands in a variety of complex nickel oxides appearing at ~720-740 nm (13500-13900 cm^{-1}), i.e. at somewhat lower energies than in our case. These differences may be due to different degree of covalence of Ni-O bonds in oxides and pyroxene structures. Note that Ito and Sone (1985) also attributed a band at 721 nm (13870 cm^{-1}) in spectrum of $[Ni(H_2O)_6]^{2+}$ to $^3A_{2g} \rightarrow {}^1E_g$ transition of Ni^{2+}.

Judging from the composition of our pyroxenes studied, Ni^{2+}, which causes the type I spectra, occupies the M1-site of the structure. This deduction well agrees with the above conclusion on a high symmetry of the octahedral structural site accommodating Ni^{2+}: as known, M1 octahedron in structures of various pyroxenes is much more regular than M2 (e.g. Burns 1993). Particularly, in the end-member $CaNiSi_2O_6$ pyroxene Ni-O distances are 2.050 Å (2), 2.059 Å (2) and 2.101 Å (2), yielding the mean value 2.070 Å, likewise Ca-O distances in CaO_8-polyhedron are 2.336 Å (2), 2.345 Å (2), 2.592 Å (2) and 2.711 Å (2) giving the mean value 2.496 Å (Ghose et al. 1987). In terms of mean-square relative deviation from the average, $\Delta' = \frac{1}{6} \cdot \sum_{1=1}^{n} [(R_i - \overline{R})/\overline{R}]^2$, where R_i is distance from the central atom to the *i*-th oxygen ion in the octahedron, $\overline{R}$ is the average bond length in Å (Brown and Shannon 1973), the Δ'-value of the M1 octahedron in the $CaNiSi_2O_6$ pyroxene structure, NiO_6, is ~0.0001, thus evidencing that indeed it is very little distorted even when compare, for instance, with the nearly regular octahedral M1 site in structures of natural orthopyroxene or clinopyroxene (diopside), ~0.0004 and ~0.0003, respectively (cf. Taran and Langer 2001).

As was already noted, unpolarized spectra of five pyroxenes, $Ni_{0.1}$ to $Ni_{0.8}$, are qualitatively very similar to each other. But due to different Ni contents and also to different thicknesses of the samples they significantly differ in the bands intensities. Besides, the energies of the spin-allowed bands *a*, *b* and *e* gradually change with Ni content (cf. e.g. spectra of $Ni_{0.3}$ and $Ni_{0.6}$ pyroxenes in Fig. 1). As seen from Fig. 3, where the energies of these three bands derived from unpolarized spectra of $Ni_{0.1}$ to $Ni_{0.8}$ pyroxenes are plotted versus the molar $CaNiSi_2O_6$ content, the bands shift linearly to higher energies with $CaNiSi_2O_6$ content thus evidencing that the dimension of the octahedral M1 site, accommodating Ni^{2+} in the pyroxene structure, decreases along the join $NaScSi_2O_6$-$CaNiSi_2O_6$. The latter is apparently due to the smaller effective octahedral radius of Ni^{2+} compared to Sc^{3+}, 0.690 Å and 0.745 Å, respectively (Shannon 1976), that leads to shortening of Ni^{2+}-O bond lengths when Ni^{2+} substitutes Sc^{3+}. This

is also consistent with the mean M1-O distances in $NaScSi_2O_6$ and $CaNiSi_2O_6$ end members, 2.102 Å (Ohashi et al. 1994) and 2.070 Å (Ghose et al. 1987), respectively, evidencing that the mean Ni^{2+}-O bond length decreases along the join $NaScSi_2O_6$ - $CaNiSi_2O_6$.

The above mentioned *a*-, *b* and *e*-band's shifts well agree with deductions of the crystal field theory, according to which energy of the first transition, $^3A_{2g} \rightarrow {}^3T_{2g}$ of $^{VI}Ni^{2+}$, i.e. the *a*-band, is a linear function and those of the two others spin-allowed transitions of Ni^{2+}, $^3A_{2g} \rightarrow {}^3T_{1g}$ and $\rightarrow {}^3T_{1g}$ (^3P), i.e. *b*- and *e*-bands, respectively, are nearly linear functions of the crystal field strength *Dq* (e.g. Sviridov et al. 1976, Marfunin 1979, Burns 1993). This in turn depends on the mean Ni-O distance $\overline{R}$ in the coordination octahedron as

$$Dq = \frac{3 < r^4 > (Z_L e^2)}{5\overline{R}^5} \qquad (1),$$

where $<r^4>$ is the mean value of the fourth power of the 3*d*-electron radius, Z_L is the effective ligand charge and *e* is the charge of electron. From this one can conclude that *Dq* and, therefore, energies of the spin-allowed bands *a*, *b* and *e*, increase, when $\overline{R}$, the mean cation-oxygen distance in the $Ni^{2+}O_6$ octahedron, decreases. Note in this connection that the energy of the spin-forbidden *c*-band in the type I spectra of different samples remains nearly invariable, ~14400 cm^{-1}. That supports its assignment to the $^3A_{2g} \rightarrow {}^1T_{2g}$ (^1D) transition of Ni^{2+}: by theory energy of this transition is nearly independent on *Dq*.

As seen from Fig. 4, where spectra of $Ni_{0.3}$ pyroxene measured at different pressures are shown, *a*-, *b*- and *e*-bands distinctly shift to higher energies with pressure. On the whole, such a behavior corresponds to their assignment to spin-allowed *dd* transitions of Ni^{2+}: since their energies are linear or nearly linear functions of the crystal field strength *Dq* (see above) and, therefore, depend on the mean Ni–O distances in the coordination octahedron (see eq. (1)), the shortening of the structural bonds at pressure should produce the shifts of the bands to higher energies. It is remarkable that intensities of the bands in question, especially, those of the *a*- and *e*-bands, noticeably decrease in the pressure range from 10^{-4} to ca. 3 GPa, then very slowly

increase under further compression to ~6 GPa. Such pressure-induced behavior very likely evidences that on the first stage of the hydrostatic compression the distortion of the $Ni^{2+}(M1)O_6$-octahedra decreases. This effect reminds in some way the pressure-induced behavior of spin-allowed dd-bands of Fe^{2+}(M2) in natural orthopyroxene (Taran and Langer 2003). The weak intensification of the bands at the second stage, at pressures growing from ca. 3 GPa to 6 GPa, may be caused by a change of spin-orbit coupling of Ni^{2+} as it was assumed in the case of spin-allowed bands of $^{VIII}Co^{2+}$ in cobalt aluminum garnet (Taran et al. 2002). In our case this effect seems relatively weak as it is superimposed on and partly compensated by the former one – increasing symmetry of the coordination octahedron.

It should be noted that the pressure induced changes in the spectrum of $Ni_{0.3}$ pyroxene are completely reversible. At least, we did not detect any noticeable hysteresis phenomena in the spectra studied.

It is interesting that the shape of the envelope, involving *b*- and *c*-bands, significantly varies with pressure (Fig. 4). This may be due to an increasing overlap of the two bands because of different pressure-induced shifts: stronger shift for the spin-allowed *b*-bands and weaker or none shift for the spin-forbidden *c*-band. Besides, such an effect may be caused by the fact that the $^3A_{2g} \rightarrow {}^3T_{1g}$ transition of Ni^{2+}, which gives rise to the *c*-band, is strongly influenced by local structural distortions, spin-orbital interaction and dynamic Jahn-Teller effect (Sviridov et al. 1976). All these factors may significantly vary with pressure.

From the shift of the *a*-band, which energy directly responds to $\Delta=10Dq$ (see above), we can calculate the value of $Ni(M1)O_6$ octahedral modulus, $k^{loc}_{Ni(M1)}$. According to Langer (1990), the mean linear polyhedral compressibility $\bar{\beta}_1 = -\frac{1}{R_0}\cdot\frac{\Delta R}{\Delta P}$, where $\Delta R = R_p - R_0 = R_0(\sqrt[5]{\Delta_0/\Delta_p} - 1)$, therefore, $\bar{\beta}_1 = \frac{1-\sqrt[5]{\Delta_0/\Delta_p}}{\Delta P}$. From this we derive the equation (2) to get the octahedral modulus, $k^{loc}_{Ni(M1)}$

$$k_{poly}^{loc} = \frac{1}{3\bar{\beta}_1} = \frac{\Delta P}{3 \cdot (1 - \sqrt[5]{\Delta_0 / \Delta_P})} \qquad (2)$$

In pyroxene $Ni_{0.3}$ the value of k_{M1}^{loc}, calculated from (2), is 85±20 GPa. This is quite commensurable with the results of a high-pressure structural study on natural diopside by Levien and Prewitt (1981). According to the latter authors, in the diopside structure the two cationic sites, M1 and M2, have similar polyhedral compressibilities, 0.95 $Mbar^{-1}$ and 0.99 $Mbar^{-1}$, or polyhedral moduli of 105 GPa and 101 GPa, respectively.

Values for the Racah parameters B of Ni^{2+}(M1) can be obtained using the formula $B = \frac{1}{3}\frac{(\nu_3 - 2\nu_1)(\nu_3 - \nu_1)}{(5\nu_3 - 9\nu_1)}$ (e.g. White et al. 1971) with energies of the *a*- and *e*-bands, ν_1 and ν_3, as derived from the high-pressure spectra in Fig. 4. As seen from Tab. 2, it gradually changes from ~919 cm^{-1} at ambient conditions to ~890 cm^{-1} at 6.18 GPa thus evidencing that the covalence of the relevant Ni^{2+}-O bonds increases under hydrostatic compression of the structure. Note, however, that these changes are rather weak when compare with the variance of B in different Ni^{2+}-bearing minerals. Indeed, as follows from Tab 5.19 in Burns (1993) B varies in a wide range from minimum value of 598 cm^{-1} in corundum to maximum, 1046 cm^{-1}, in M1 site of enstatite. In the free Ni^{2+} ion the B-value is 1115 cm^{-1}. It means that in the pyroxene studied the so-called nephelauxatic ratio, $\beta = B/B_{free}$, of Ni^{2+}(M1) varies in the pressure range 10^{-4}-6.18 GPa from 0.82 to 0.80, whereas in different minerals at ambient conditions it varies from 0.54 to 0.94. From this one may conclude that the covalence of Ni–O-bonding in the M1 site of the pyroxene studied changes relatively weakly with pressure. It should be noted that Langer et al. (1997) and Taran et al. (2007) detected no reliably fixed pressure dependence of the B-parameter in the Cr^{3+}-bearing garnet, uvarovite $Ca_3Cr_2(SiO_4)_3$. This may be due to the fact that spin-allowed bands of Cr^{3+} in the uvarovite spectrum are much broader than those of Ni^{2+} in the pyroxenes studied here. This hinders precise determination of Cr^{3+} band positions in high-pressure spectra and, thus, prevents the observation of a very like, but weak pressure effect to B-parameter of Cr^{3+}.

Due to the appearance of several extra bands (even more than in the unpolarized spectrum in Fig. 1), the type II polarized spectrum in Fig. 5 considerably differs from that of type I in Fig. 2. In addition to the bands *a* to *e*, there are three extra bands designated in Fig. 5 by their energies, 10400, 18200 and 19600 cm^{-1}. By intensity they are quite commensurable with the former *a*- to *e*-bands. From the polarized spectra it is clearly seen that the highest energy band around 24000 cm^{-1} consists of two components, with maxima at ~23000 and ~24500 cm^{-1}, which are of different intensity ratio in different polarizations.

The set of four bands *a* to *e* in the spectrum of $Ni_{1.0}$ pyroxene (Fig. 5) is doubtless of the same nature as in the other samples studied, $Ni_{0.1}$ to $Ni_{0.8}$, i.e. caused by Ni^{2+} in M1 site of the structure (see above). Moreover the energies of the three spin-allowed bands of Ni^{2+}(M1) *a*, *b* and *e* derived by the curve resolution (see below), perfectly fit the concentration dependences in Fig. 2. We assigned here the higher energy component at ~24500 cm^{-1} of the doublet *e*-band to Ni^{2+}(M1) and the lower energy component at ~23000 cm^{-1} to Ni^{2+} at M2. It is remarkable that the former value, ~24500 cm^{-1}, of the *e*-band assigned to the $^3A_{2g} \rightarrow {}^3T_{1g}$ (^3P) transition of Ni^{2+}(M1), as well as that of the $^3A_{2g} \rightarrow {}^3T_{2g}$ band, ~8410 cm^{-1} (Fig. 5), is in perfect correspondence with energies of the respective bands in power reflectance spectrum of synthetic $CaNiSi_2O_6$ diopside, 24500 cm^{-1} and 8400 cm^{-1}, studied by White et al. (1971).

Judging from the shape, energies and intensity of the extra bands at 23000, 19600, 18200 and 10300 cm^{-1} in Fig. 5 it is quite reasonable to assume that they belong, together with the extra band around 5650 cm^{-1} (Fig. 1), to electronic transitions of Ni^{2+} in other than M1 site of the pyroxene structure, namely, in M2. In addition to the microprobe data showing up to 0.067 apfu. of Ni in the M2 site of the structure substituting Ca^{2+} (Tab. 1), there are several other reasons in favor of such an interpretation. First, it is very unlikely that the extra bands in the spectrum of $Ni_{1.0}$ pyroxene are caused by Ni^{3+} since the synthesis conditions, including oxygen fugacity, were practically the same for all six synthesis runs (Ohashi 1977). Therefore, there was no reason for Ni to occur in the end-member pyroxene in the oxidation state different from the other

samples. Besides, the spectrum in Fig. 5 significantly differs from that of synthetic nickel-doped corundum, α-Al_2O_3: Ni^{3+} (e.g. Sviridov et al. 1976), which, as far as we are aware, is the only optical spectrum of Ni^{3+} (d^7-configuration) so far established in oxygen-based crystals. Note that Solntsev et al. (2006) reported some bands in spectra of synthetic Ni-doped beryls as caused by Ni^{3+}. However, these bands are strongly overlapped with intense bands of Ni^{2+} and their assignment to Ni^{3+} seem for us rather questionable.

Of course, Ni^{2+}, which possesses a strong crystal field stabilization energy effect (e.g. Burns 1993), hardly enters the tetrahedral Si-site of the structure[2]. Thus, we assume that a small portion of Ni^{2+} is located at M2, a largely distorted polyhedron of variable coordination number. The strong distortion may explain that in our $Ni_{1.0}$ pyroxene even a small portion of Ni^{2+}(M2) cause spin-allowed absorption bands of appreciable intensities, quite comparable to those of Ni^{2+}, which completely fills the M1-site of the structure. Such a phenomenon was also observed for Fe^{2+} bearing clinopyroxenes (e.g. Taran and Langer 2001). Also, due to the low symmetry and strong distortion of the M2 polyhedron all absorption bands should undergo a relatively strong splitting and, because of larger dimension of the site and, thus, relatively small *Dq*, their barycenters should be shifted to lower energies compared to the respective bands of Ni^{2+}(M1) as in the case of Fe^{2+}-bearing clinopyroxene (Taran and Langer 2001).

The actual coordination number of Ni^{2+}(M2) is not defined. Although Ni^{2+} substitutes Ca^{2+} in distorted eight-fold coordination it is not granted that the geometry and coordination number of Ni^{2+}-centered M2 polyhedra are retained. For several representative clinopyroxenes a significant residual electron density, centred close to the M2 sites, has been inferred from X-ray structure refinement. According to Rossi et al. (1987) this phenomenon is caused by an off-centre displacement of the relatively small sized cations within the M2 polyhedron (like Ni^{2+} in our case which substitutes larger Ca^{2+} (r_{oct} is 0.69 Å and 1.00 Å, respectively (Shannon 1976)). Ohashi et al. (2003) refined the crystal structure of $(Ca_{0.97},Mn_{0.03})MnSi_2O_6$ clinopyroxene

[2] Tejedor-Tejedor et al. (1983) attributed some features in diffuse reflectance spectra of nickel-bearing phyllosilicates to Ni^{2+} in four-fold coordination replacing Si^{4+}. However, latter this attribution was discriminated by Manceau and Calas (1987), who found "no spectroscopic support of tetrahedrally coordinated Ni in phyllosilicates".

($r_{oct}^{Mn^{2+}} = 0.83$ Å) using a split atom model for the M2 site and clarified that the off-centre displacement results in the four coordinated character of Mn(M2)O_8 polyhedron. Particularly, they found that at such substitution four shorter metal-oxygen distances in M2O_8 become even shorter, whereas four longer bonds become longer. Likewise, a similar effect may take place in the case of (Ca, Ni)$NiSi_2O_6$ having even larger difference in substituting ions' size (see above). However, judging from the energies of the extra bands in spectrum of $Ni_{1.0}$ pyroxene (Figs. 1, 5), if such an effect does take place, the coordination number should rather be regarded as close to a large distorted octahedron than to a tetrahedron. Indeed, taking into consideration that $Ä_{tetr} = -\frac{4}{9} Ä_{oct}$ (e.g. Burns 1993), the energy of the lowest-energy band is expected to be around 3380 cm^{-1} ($\frac{4}{9} \times 7610$ cm^{-1} (cf. Tab. 2)), whereas it appears at ~5650 cm^{-1} (Fig. 1). On this account, the most intense extra bands at 23000 cm^{-1} and 19600 cm^{-1} may be attributed to the split $^3A_{2g} \rightarrow {}^3T_{1g}(^3P)$ transition of Ni^{2+}(M2) in octahedral coordination. The latter band, at 19600 cm^{-1}, is apparently of asymmetric shape. Therefore, it should be a combination of, at least, two bands. As result, we assume that there are three transitions to the $^3T_{1g}$ (^3P) level of octahedral Ni^{2+}(M2) which arise from the split of the level by the low symmetry crystal field. Then, by analogy, the bands at 10370 cm^{-1} is probably a component caused by the split of the $^3A_{2g} \rightarrow {}^3T_{1g}$ (^3F) transition, its high-energy counterpart(s) being overlapped by the more intense *b*-band of Ni^{2+}(M1). The shape of the resulting band in the spectrum of $Ni_{1.0}$ pyroxene (Fig. 5) obviously differs from that of the respective *b*-band in type I spectra of other pyroxenes (cf. Fig. 2) which supports this assumption. The lowest energy band, $^3A_{2g} \rightarrow {}^3T_{2g}$, is, as mentioned above, aside of the spectral range studied, i.e. at ~5650 cm^{-1} (cf. Fig. 1). A vague shoulder at 18200 cm^{-1} can be one of the spin-forbidden transitions of Ni^{2+}(M2), most likely, $^3A_{2g} \rightarrow {}^1A_{1g}$ (^1G).

In general, the proposed interpretation is in agreement with the pressure-induced behavior of the absorption bands in the type II spectrum of $Ni_{1.0}$ pyroxene. As seen from Fig. 6, with

increasing pressure all bands of Ni^{2+}, those caused by Ni^{2+}(M1), as well as those assigned to Ni^{2+}(M2), quite expectedly (cf. Fig. 4) shift to higher energies due to shortening of Ni^{2+}(M1)–O and Ni^{2+}(M2)–O bonds in the coordination polyhedra and, thus, because of an increase of the crystal field strength *Dq* (see eq. 1). As has already been noted, this agrees with deductions of the crystal field theory according to which energies of all spin-allowed transitions of Ni^{2+} linearly or nearly linearly depends on the crystal field strength *Dq*.

The intensities of the bands caused by different Ni^{2+}-centers, Ni^{2+}(M1) and Ni^{2+}(M2), respond to pressure in quite different ways. It seems certain that intensities of the bands assigned to the electronic spin-allowed transitions of Ni^{2+}(M1), relatively weakly depend on P, whereas the bands caused by Ni^{2+}(M2), i.e. the extra bands, change in intensity much stronger. Note also that due to a significant change of the shape of the transmittance window in the visible range of the spectra (Fig. 6), the color of the $Ni_{1.0}$ pyroxene gradually changes from a weak greenish-yellow at ambient pressure to a dark emerald-green at ~10 GPa in difference to $Ni_{0.3}$ pyroxene which color remains nearly unchanged with pressure.

The differences in pressure induced behavior of the bands attributed to Ni^{2+}(M1) and Ni^{2+}(M2) in spectrum of $Ni_{1.0}$ pyroxene are better seen from the results of the curve fitting procedure. Two curve resolved spectra measured at ambient pressure and at 10.48 GPa are shown in Fig. 7. The extra bands of Ni^{2+}(M2) are marked as filled by gray. As was expected before, the $^3A_{2g} \rightarrow {}^3T_{1g}(^3P)$ transition of Ni^{2+}(M2) is obviously split into three bands. However, the result of the curve resolution in the range of *b*-band of Ni^{2+}(M1) at both the ambient pressure and at 10.48 GPa looks rather questionable. Also, the energy of the weak *d*-band is much lower, around 19000 cm^{-1}, than it is obtained for $Ni_{0.3}$, ~20800 cm^{-1} (cf. Fig. 2). Nevertheless, it is clearly seen that both sets of bands, the *a*-, *b*- and *e*-bands, caused by Ni^{2+}(M1) and the extra bands of Ni^{2+}(M2) shift to higher energies with increasing pressure. From the shift of the *a*-band of Ni^{2+}(M1), caused by the $^3A_{2g} \rightarrow {}^3T_{2g}$ transition, the value of the local octahedral compression modulus of Ni^{2+}(M1)O_6 octahedra, $k^{loc}_{Ni(M1)}$, is evaluated using expression (2) as ~150±25 GPa,

which is noticeably larger than in $Ni_{0.3}$ pyroxene, 85±20 GPa (see above). Perhaps, this is due to the smaller size and, thus, a stiffer character of $Ni(M1)O_6$ octahedron in the end member $N_{1.0}$ pyroxene compared with $Ni_{0.3}$. Unfortunately, we were unable to evaluate in such a way the compression modulus of the Ni(M2) polyhedron as the band of the $^3A_{2g} \rightarrow {}^3T_{2g}$ transition of Ni^{2+}(M2) used for such calculations, appears at 5650 cm^{-1} (cf. Fig. 1) which is beyond the spectral range studied in the high-pressure spectroscopic experiments.

As seen from Figs. 6 and 7, intensities of the spin-allowed bands, attributed to Ni^{2+}(M1) and Ni^{2+}(M2) do display different pressure-induced behavior. As noted above, within the uncertainty of the high-pressure spectroscopic measurements and the curve fitting procedure the intensities of the *a*-, *b*- and *e*-bands of Ni^{2+}(M1) change relatively weakly. This implies a relatively weak pressure-induced effect to the distortion of the M1 octahedron. On the contrary to the Ni^{2+}(M1) bands, intensities of the three bands, derived from the split $^3A_{2g} \rightarrow {}^3T_{1g}(^3P)$ transition of Ni^{2+}(M2) (see above), strongly decrease. This effect was already observed on spin-allowed bands of Fe^{2+}(M2) in natural iron-bearing orthopyroxene by Taran and Langer (2003). Also, the splitting between the three components derived from the split of the $^3A_{2g} \rightarrow {}^3T_{1g}(^3P)$ transition significantly decreases, so that the energy gap between the utmost bands of the triplet (Fig. 7) decreases from ca. 3200 cm^{-1} at ambient pressure to ca. 2580 cm^{-1} at 10.48 GPa. These all evidence that pressure strongly decreases the distortion of the Ni^{2+}(M2)-centered polyhedra resulting in a decrease of the $^3T_{1g}(^3P)$-level splitting and diminishing of the Laporte selection rule relaxation for the $^3A_{2g} \rightarrow {}^3T_{1g}(^3P)$ transition and, thus, weakening of the corresponding absorption bands. It is very likely that a similar shift of the high energy component band derived from the split of the $^3A_{2g} \rightarrow {}^3T_{1g}$ transition of Ni^{2+}(M2) causes a noticeable pressure-induced change of the shape of the complex band around 15000 cm^{-1}, which is regarded as a combination of the $^3A_{2g} \rightarrow {}^3T_{1g}$ band of Ni^{2+}(M2) and the *b*- and *c*-band of Ni^{2+}(M1). On the other hand, it is difficult to explain the relatively strong decrease of the splitting between the two bands caused by $^3A_{2g}$

$\rightarrow {}^3T_{1g}$ transition of Ni^{2+}(M2) as revealed by the curve fitting procedure (Fig. 7). This results in a weak pressure induced shift of the barycenter of the two bands from ca. 12775 cm^{-1} at ambient pressure to only 12950 cm^{-1} at 10.48 GPa, which sums up to only 175 cm^{-1}. Meanwhile, according to the curve fitting, the maximum of the *b*-band of Ni^{2+}(M1), also originating from ${}^3A_{2g} \rightarrow {}^3T_{1g}$ transition of Ni^{2+}, shifts under these conditions from ~13300 to ~15900 cm^{-1}, i.e. the shift is as large as 2600 cm^{-1}, more than one order of magnitude stronger that in the former case. Perhaps, all these discrepancies are due to the complex character of this latter band of Ni^{2+}(M1). As was already noted, many investigators attribute its splitting and a complicated shape in different crystal structures to a dynamic Jahn-Teller effect, low symmetric crystal field and spin-orbital coupling (e.g. Sviridov et al. 1976). Some intensification of this band at high pressures, > ca. 5 GPa, together with significant change of its shape (Fig. 6), may be due, at least partly, to these factors.

To finish the discussion of pressure-induced effects on the absorption spectrum of $Ni_{1.0}$ pyroxene we should emphasize that within the uncertainty of the experiment they are completely reversible without any noticeable hysteresis, i.e. are, in this respect, quite similar to $Ni_{0.3}$ pyroxene.

It is quite obvious that the nickel content in the pyroxenes studied is mostly controlled by Na^+ to Ca^{2+} substitution which provides the charge balance at the heterovalent $Sc^{3+} \rightarrow Ni^{2+}$ substitution. As noted before, in the end member $Ni_{1.0}$ pyroxene some surplus amount of Ni^{2+}, 0.067 apfu. (Tab. 1), enters the M2 site, substituting Ca^{2+}. This has also be confirmed by optical spectroscopy and one can roughly estimate the Ni^{2+}(M2) content from the absorption spectrum under the assumption that the molar absorptivity, ε, of Ni^{2+}(M2) and Ni^{2+}(M1) spin-allowed bands is of the same orders of magnitude as, respectively, the molar absorptivity of Fe^{2+}(M1) and Fe^{2+}(M2) in natural orthopyroxenes. Thus, according to Goldman and Rossman (1978), ε-value of the two spin-allowed bands of Fe^{2+}(M2) at ~11000 cm^{-1} and ~5000 cm^{-1}, originating from the

split of the ${}^5T_{2g} \rightarrow {}^5E_g$ transition and averaged over three polarizations α, β and γ, is around 16.2 and 4.6, respectively. The ε-value of the γ-polarized band at 8600 cm^{-1}, attributed to Fe^{2+}(M1), is estimated to be 4.6. Averaged over three polarizations this results in ~1.5. As seen from Fig. 7a, overall intensity of the bands caused by Ni^{2+}(M2) is about two times lower than those caused by Ni^{2+}(M1). From this we can estimate that Ni^{2+} content in M2 should be from 25 to 6 times lower than that in M1. Note, that by the microprobe analysis this value is ~15, just within the above range.

By partitioning between two cationic sites M1 and M2 in the pyroxene structure, Ni^{2+} significantly differs from Cr^{3+}, which occupies solely the M1 site (Burns 1993). However, one should remember that Ni^{2+} substituting Ca^{2+} in M2 does not need any charge compensation, whereas Cr^{3+} needs.

Taking into consideration the strong crystal field stabilization energy effect of Ni^{2+} one may reasonably assume that the preference of Ni^{2+} for the smaller octahedral M1 site in $CaNiSi_2O_6$ pyroxene is caused by this circumstance. If so, the situation may noticeably change at high pressures, where M2 undergoes a larger compression as the M1. Taking into account that Ni^{2+} distribution over the two sites is, at least partly, regulated by the crystal field stabilization energy effect, this implies that at high pressures the Ni^{2+} partitioning into M2 may be higher than at ambient pressure.

Acknowledgements

We are thankful to two anonymous reviewers which comments and suggestions helped to improve the manuscript.

References

Boström D (1987) Single-crystal X-ray diffraction studies of synthetic Ni-Mg olivine solid solution. Amer Mineral 72: 965-972

Brown ID and Shannon RD (1973) Empirical bond-strength-bond-length curves for oxides. Acta Cryst A29: 266-282

Burns RG (1993) Mineralogical applications of crystal field theory. 2nd ed. Cambridge University Press, Cambridge

Fukunaga O, Yamaoka S, Endo T, Akaishi M, Kanda H (1979) Modification of belt-like high-pressure apparatus. High- Pressure Sci Technol 1: 846-852

Garsche M, Langer K (1994) Equilibrium and kinetics of cation distribution in Ni-Mg-olivine from structure refinements and microspectrometry. In: Putnis A, ed, Kinetics processes in minerals and ceramics (MINC). Proceedings of an ESF Workshop on kinetics of cation ordering. Cambridg, 5 pp.

Ghose S, Wan C, Okamura FP (1987) Crystal structures of $CaNiSi_2O_6$ and $CaCoSi_2O_6$ and some crystal-chemical relations in *C2/c* clinopyroxenes. Amer Mineral 72: 375-381

Goldman DS, Rossman GR (1978) Determination of quantitative cation distribution in orthopyroxenes from electronic absorption spectra. Phys Chem Minerals 4: 43-55

Hu X, Langer K, Bostrom D (1990) Polarized electronic absorption spectra and Ni-Mg partitioning in olivines $(Mg_{1-x}Ni_x)_2[SiO_4]$. Eur J Mineral 2: 29-41

Ito H, Sone K (1985) On the assignment of band II in the electronic spectrnm of $[Ni(H_2O)_6]^{2+}$. Bull Chem Soc Jpn 58: 2703-2702

Langer K (1990) High pressure spectroscopy. In: Monttana A, Burragato F (eds.) Absorption Spectroscopy in Mineralogy, p 228-284. Elsevier

Langer K (2000) Another look through the microscope – locally resolved electronic absorption spectra of silicate minerals measured in a microscope-spectrometer. J Czech Geol Soc 45: 37-62

Langer K., Taran M.N., Platonov A.N. (1997) Compression moduli of Cr^{3+}-centered octahedra in a variety of oxygen-based rock-forming minerals. Phys. Chem. Minerals 24: 109-114

Levien L, Prewitt CT (1981) High-pressure structural study of diopside. Am Mineral 66: 315-323

Manceau A, Calas G, Decarreau A (1985) Nickel-bearing clay minerals: 1. Optical spectroscopic study of nickel crystal chemistry. Clay Minerals 20: 367-387

Manceau A, Calas G (1987) Absence of evidence for Ni/Si substitution in phyllosilicates. Clay Minerals 22: 357-362

Marfunin AS (1979) Physics of minerals and inorganic materials: an introduction. Berlin-NY, Springer-Verlag

Ohashi H (1988) Unit cell dimensions of the $NaScSi_2O_6$-$CaNiSi_2O_6$ series pyroxenes formed at atmospheric pressure. J Min Petr Econ Geol 83: 440-442

Ohashi H, Osawa T, Kimura M (1997) Immiscibility phenomena in the $NaScSi_2O_6$ - $CaNiSi_2O_6$ pyroxene system at 6 GPa pressure. In: Geochemical Studies on Synthetic and Natural Rock Systems. Gupta AK, Onuma K, Arima M (eds), New Delhi, Allied Publishers LTD, 42-47

Ohashi H, Osawa T, Sato A (1994) Structure of $NaScSi_2O_6$. Acta Cryst C50: 838-840

Ohashi H, Osawa T, Sato A (2003) Crystal structures of (Na, Ca)(V, Mn)Si_2O_6 pyroxenes, In: X-ray study on Si-O bonding (Ohashi H ed.) Maruzen, Tokyo, ISBN 4-89630-094-7, 59-71

Ottonello G, Della Giusta A, Molin GM (1989) Cation ordering in Ni-Mg olivines. Amer Mineral 74: 411-421

Rossi G, Oberti R, Dal Negro A, Molin GM, Mellini M (1987) Residual electron density at the M2 site in C2/c clinopyroxenes: Relationships with bulk chemistry and sub-solidus evolution. Phys Chem Minerals 14: 514-520

Rossman GR, Shannon RD, Warring RK (1981) Origin of the yellow color of complex nickel oxides. Journal of Solid State Chemistry 39: 277-287

Shannon RD (1976) Revised effective ionic radii and systematic sdtudies of interatomic distances in halides and chaleogenides. Acta Cryst A32: 751-767

Solntsev VP, Tsvetkov EG, Alimpiev AI, Mashkovtsev RI (2006) Coordination and valent state of nickel ions in beryl and chrysoberyl crystals. Phys Chem Minerals 33: 300-313

Sviridov DT, Sviridova RK, Smirnov YuF (1976) Optical spectra of transition metal ions in crystals. Moscow, Nauka (in Russian)

Taran MN, Langer K (2001) Electronic absorption spectra of Fe^{2+} ions in oxygen-based rock-forming minerals at temperatures between 297 and 600 K. Phys Chem Minerals 28: 199-210

Taran MN, Langer K (2003) Single-crystal high-pressure electronic absorption spectroscopic study of natural orthopyroxenes. Eur J Mineral 15: 689-695

Taran MN, Langer K., Koch-Müller M (2007) Pressure dependence of color of natural uvarovite: the barochromic effect. Phys Chem Minerals (in press)

Taran MN, Langer K, Geiger CA (2002) Single-crystal electronic absorption spectroscopy of synthetic chromium-, cobalt-, and vanadium-bearing pyropes at different temperatures and pressures. Phys Chem Minerals 29: 362-368

Taran MN, Langer K, Platonov AN, Indutny VV (1994) Optical absorption investigation of Cr^{3+} ion-bearing minerals in the temperature range 77-797 K. Phys Chem Minerals 21:360-372

Tejedor-Tejedor M.I., Anderson MA, Herbillon AJ (1983) An investigation of the coordination number of Ni^{2+} in nickel bearing phyllosilicates using diffuse reflectance spectroscopy. J Solid State Chem 50: 153-162

Tröger VE (1968) Optical identification of rock-forming minerals. Moscow, Nedra Publisher (in Russian)

White WB, McCarthy GJ, Scheetz BE (1971) Optical spectra of chromium, nickel, and cobalt-containing pyroxenes. Am Mineral 56: 72-89

Tab. 1. Results of microprobe analysis of five synthetic clinopyroxenes studied (averaged over five measurements in different points of each sample).

Intended composition	Oxides, wt.%						Cations, apfu.					
	Na_2O	SiO_2	CaO	Sc_2O_3	NiO	Sum	Na	Si	Ca	Sc	Ni	Sum
$(Na_{0.9}, Ca_{0.1})(Sc_{0.9}, Ni_{0.1})Si_2O_6$	11.63	53.97	2.56	26.87	3.37	98.43	0.847	2.026	0.103	0.879	0.102	3.958
$(Na_{0.8}, Ca_{0.2})(Sc_{0.8}, Ni_{0.2})Si_2O_6$	10.05	52.76	5.49	23.18	7.06	98.57	0.744	2.014	0.225	0.771	0.217	3.972
$(Na_{0.7}, Ca_{0.3})(Sc_{0.7}, Ni_{0.3})Si_2O_6$	9.24	52.09	7.05	21.30	9.43	99.14	0.688	2.002	0.291	0.713	0.292	3.987
$(Na_{0.4}, Ca_{0.6})(Sc_{0.4}, Ni_{0.6})Si_2O_6$	4.45	50.30	14.36	11.22	19.20	99.56	0.344	2.006	0.614	0.390	0.616	3.971
$CaNiSi_2O_6$	0.01	47.54	20.42	0.00	31.46	99.45	0.001	2.004	0.922	0.000	1.067	3.995

Table 2. Energies of the spin-allowed *a*- and *e*-bands, ν_1 and ν_3, respectively, and the Racah parameter *B* of Ni^{2+}(M1) in $Ni_{0.3}$ pyroxene at different pressures.

P, GPa	ν_1, cm^{-1}	ν_3, cm^{-1}	*B*, cm^{-1}
10^{-4}	7610	23830	919
10^{-4} *)	7640*)	23760*)	911
2.95	8100	24320	901
4.69	8390	24720	899
6.18	8600	24930	890

*) Measured after releasing the highest pressure, 6.18 GPa, to atmospheric, 10^{-4} GPa.

Figure captions

Fig. 1. Typical unpolarized spectra of pyroxene studied. $Ni_{0.3}$ and $Ni_{0.6}$ pyroxenes represent spectra of the type I. $Ni_{1.0}$ pyroxenes represents spectrum of the type II (see text).

Fig. 2. **a** - Polarized spectra of $Ni_{0.3}$ pyroxene (a section cut out parallel the crystal elongation); **b** - result of curve resolution of the polarized spectrum of $Ni_{0.3}$ pyroxene.

Fig. 3. Energies of three spin-allowed bands *a*, *b* and *e* of Ni^{2+}(M1) ions in unpolarized type I spectra of pyroxenes a function of the $CaNiSi_2O_6$ molar content (black symbols). Energies of the three bands derived by the curve fitting procedure from spectrum of the end-member $Ni_{1.0}$ of type II are shown by the empty circles.

Fig. 4. Spectra of $Ni_{0.3}$ pyroxene measured at different pressures.

Fig. 5. Polarized spectra of type II of $Ni_{1.0}$ pyroxene (a section cut out parallel the crystal elongation). The bands of Ni^{2+}(M1) are labeled as *a*, *b*, *c* and *e*. The extra bands caused by Ni^{2+}(M2) are marked by energies of their maxima.

Fig. 6. Spectra of the end member $Ni_{1.0}$ pyroxene measured at different pressures.

Fig. 7. Curve-resolved spectra of $Ni_{1.0}$ pyroxene measured at two different pressures: **a** – ambient pressure; **b** – 10.48 GPa. Spin-allowed transitions of Ni^{2+}(M1) are designated as *a*-, *b*- and *e*-bands. The bands attributed to the spin-allowed transitions of Ni^{2+}(M2) are shown by the filled Gaussians.

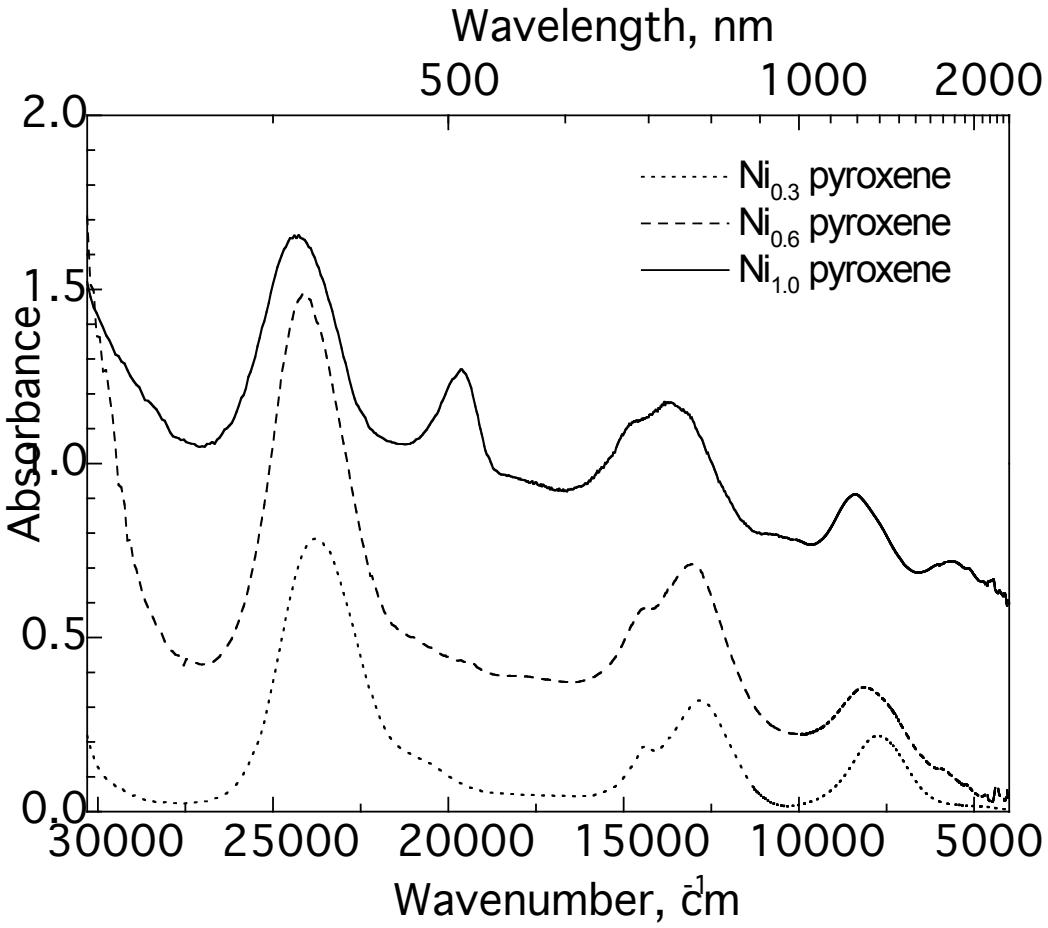

Fig. 1. Typical unpolarized spectra of pyroxene studied. $Ni_{0.3}$ and $Ni_{0.6}$ pyroxenes represent spectra of the type I, $Ni_{1.0}$ pyroxenes represents spectrum of the type II (see text).

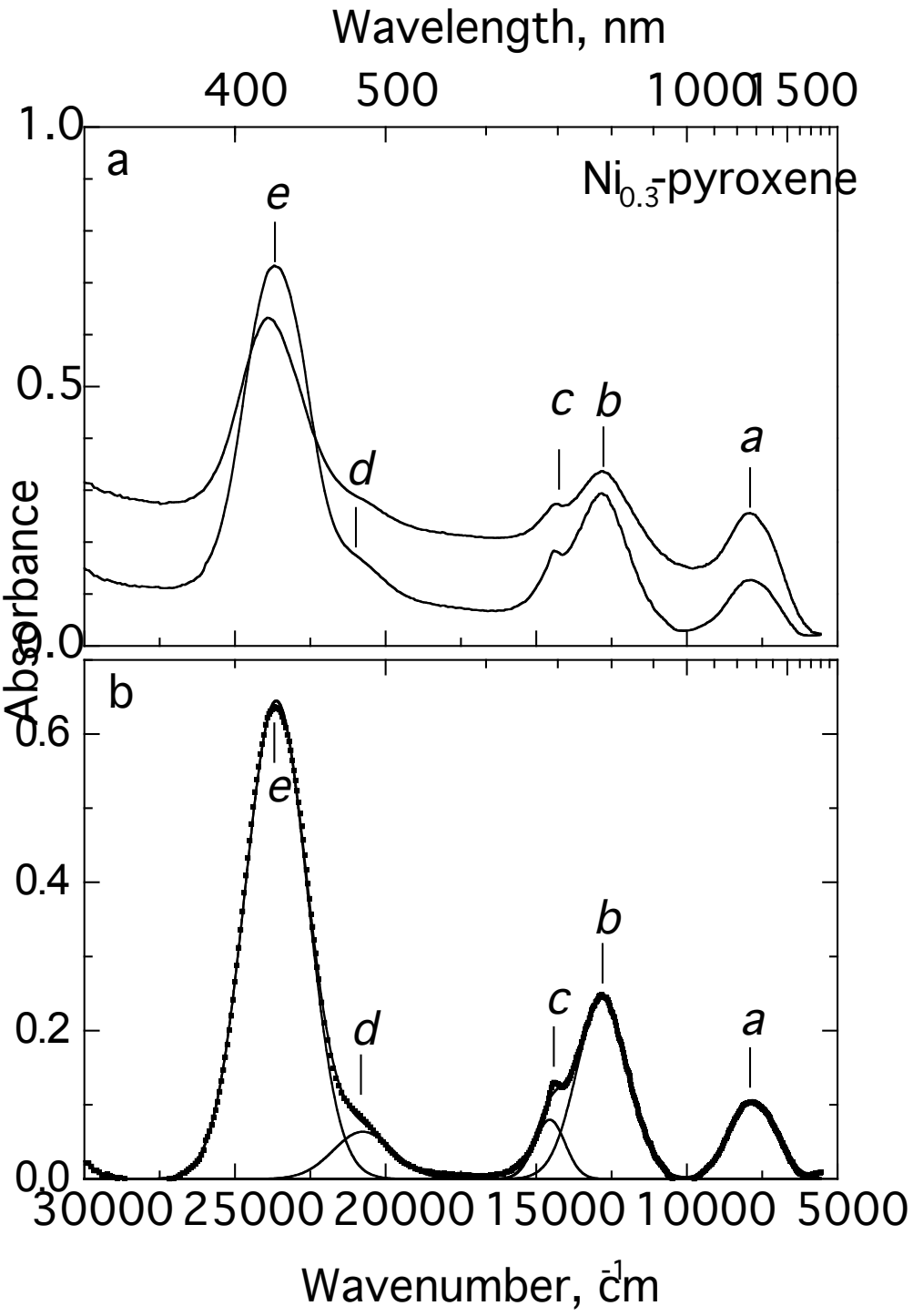

Fig. 2. **a** - Polarized spectra of $Ni_{0.3}$ pyroxene (section cut out parallel the crystal elongation); **b** - result of curve resolution of the polarized spectrum of $Ni_{0.3}$ pyroxene.

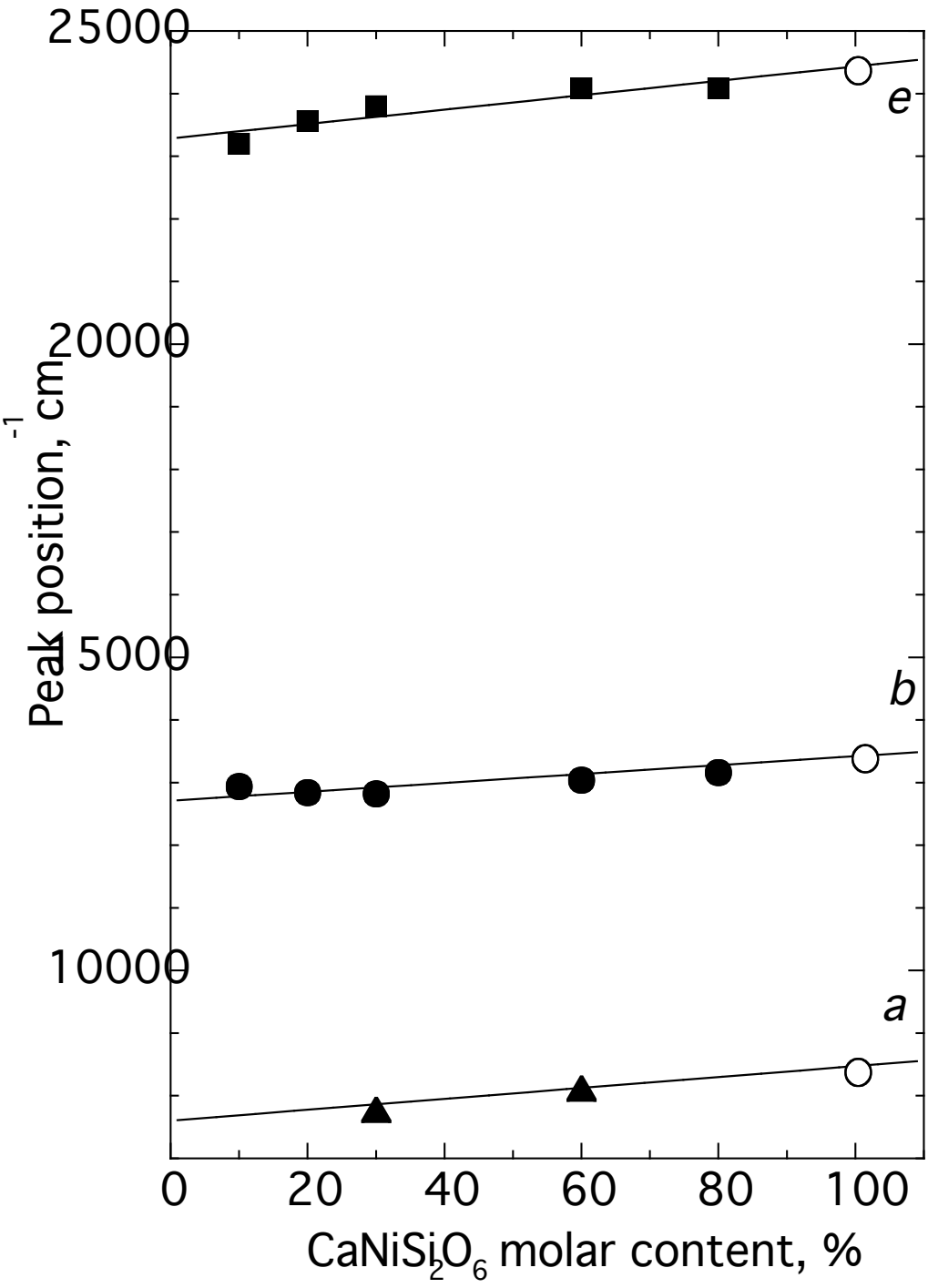

Fig. 3. Energies of three spin-allowed bands *a*, *b* and *e* of Ni^{2+}(M1) ions in unpolarized type I spectra of pyroxenes a function of the $CaNiSi_2O_6$ molar content (black symbols). Energies of the three bands derived by the curve fitting procedure from spectrum of the end-member $Ni_{1.0}$ of type II are shown by the empty circles.

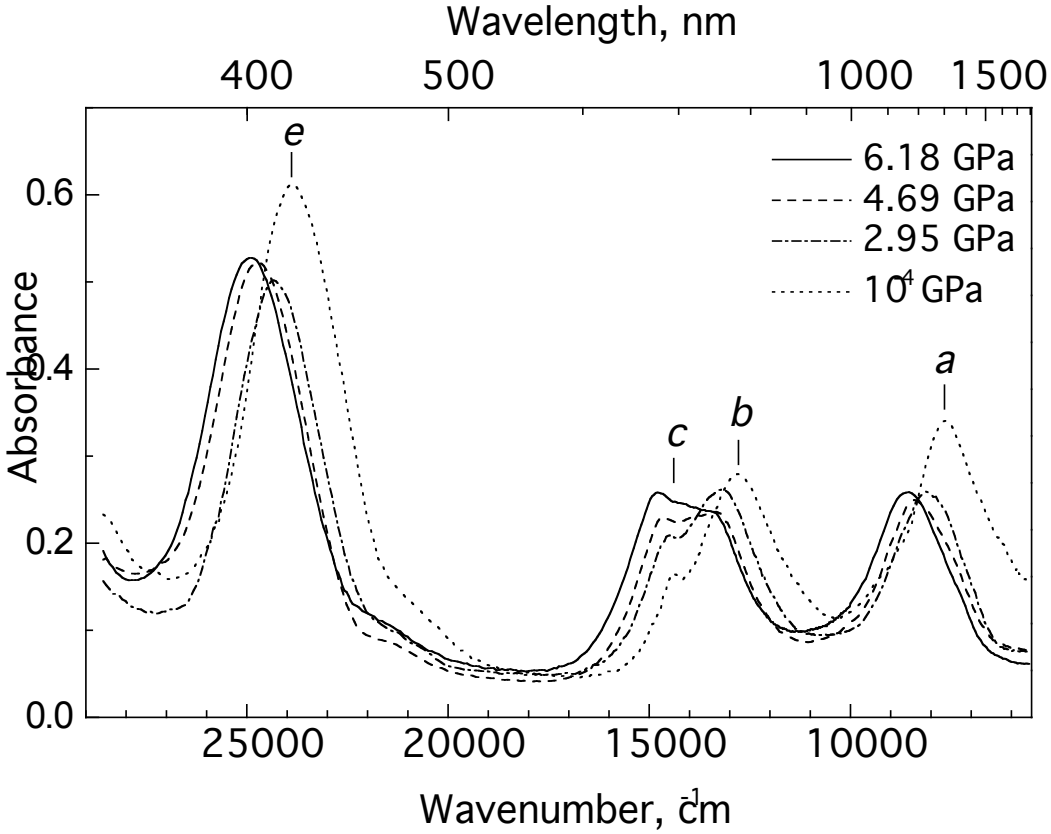

Fig. 4. Spectra of $Ni_{0.3}$ pyroxene measured at different pressures.

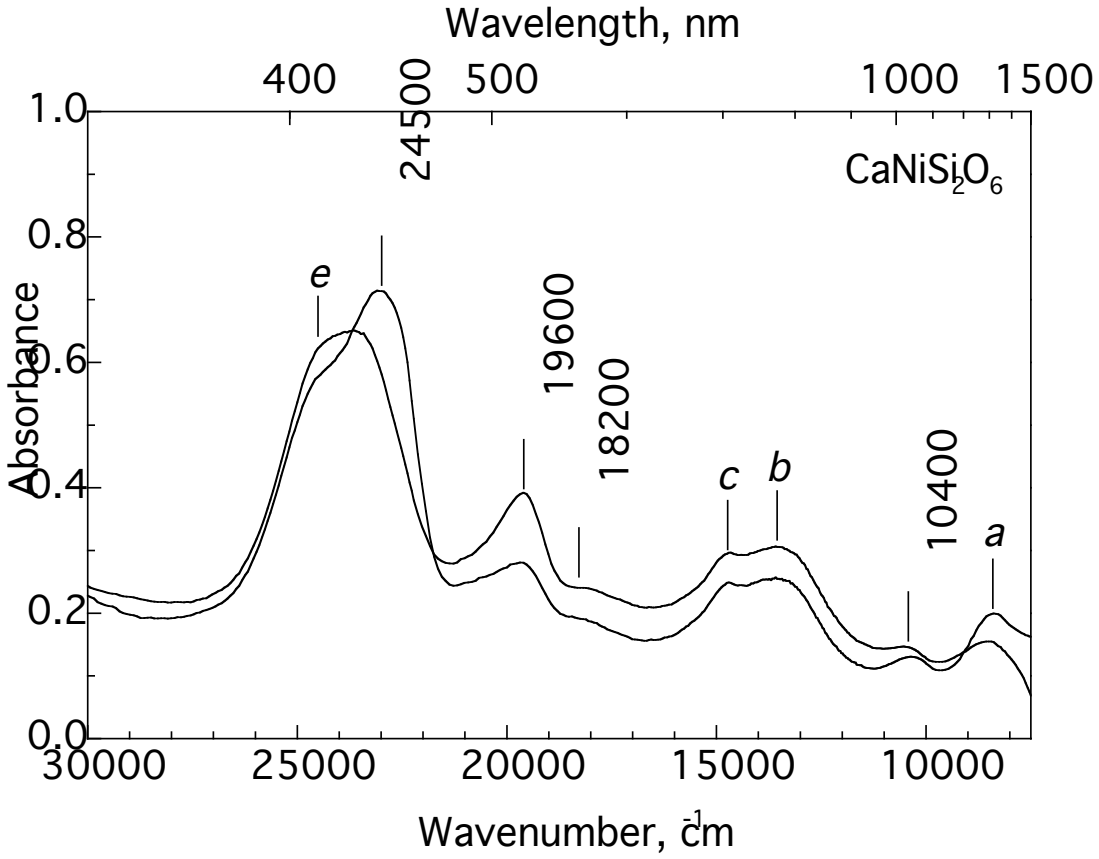

Fig. 5. Polarized spectra of type II of $Ni_{1.0}$ pyroxene (a section cut out parallel the crystal elongation). The extra bands of Ni^{2+}(M2) are marked by energies of their maxima. The "regular" bands *a*, *b*, *c* and *e* of Ni^{2+}(M1) are also shown.

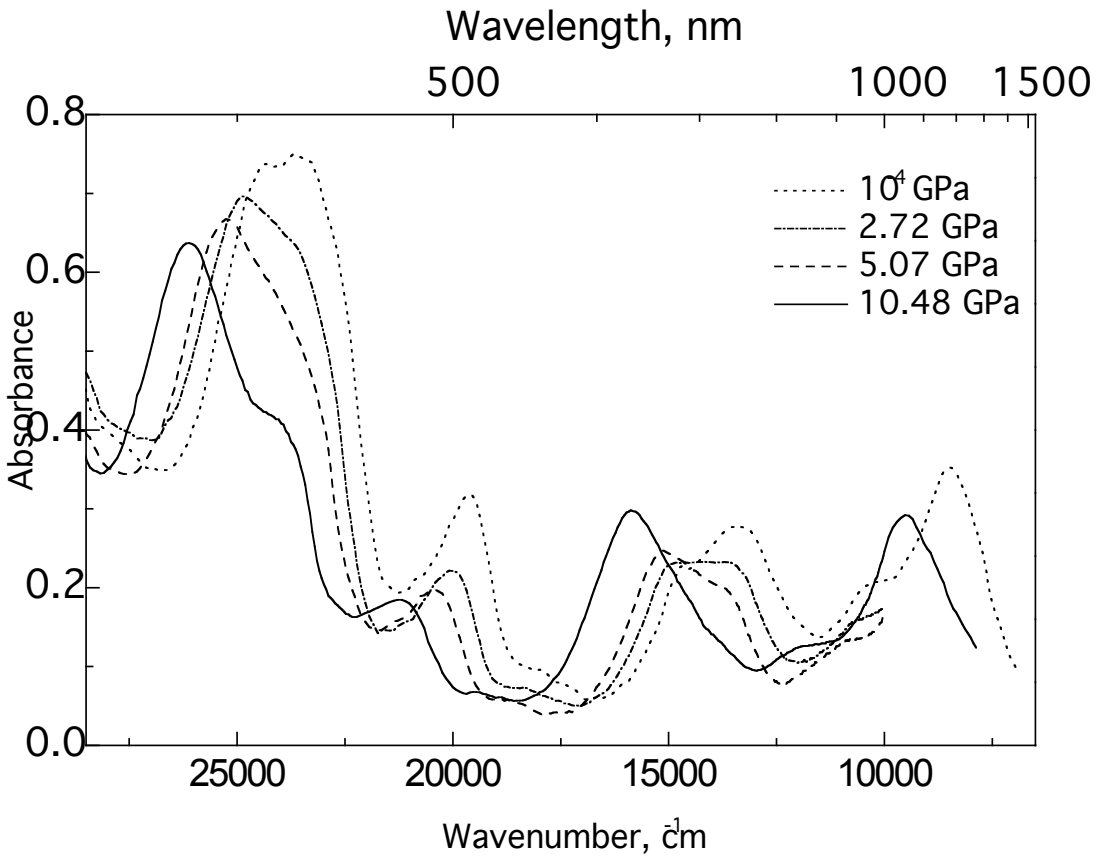

Fig. 6. Spectra of the end member $Ni_{1.0}$ pyroxene measured at different pressures.

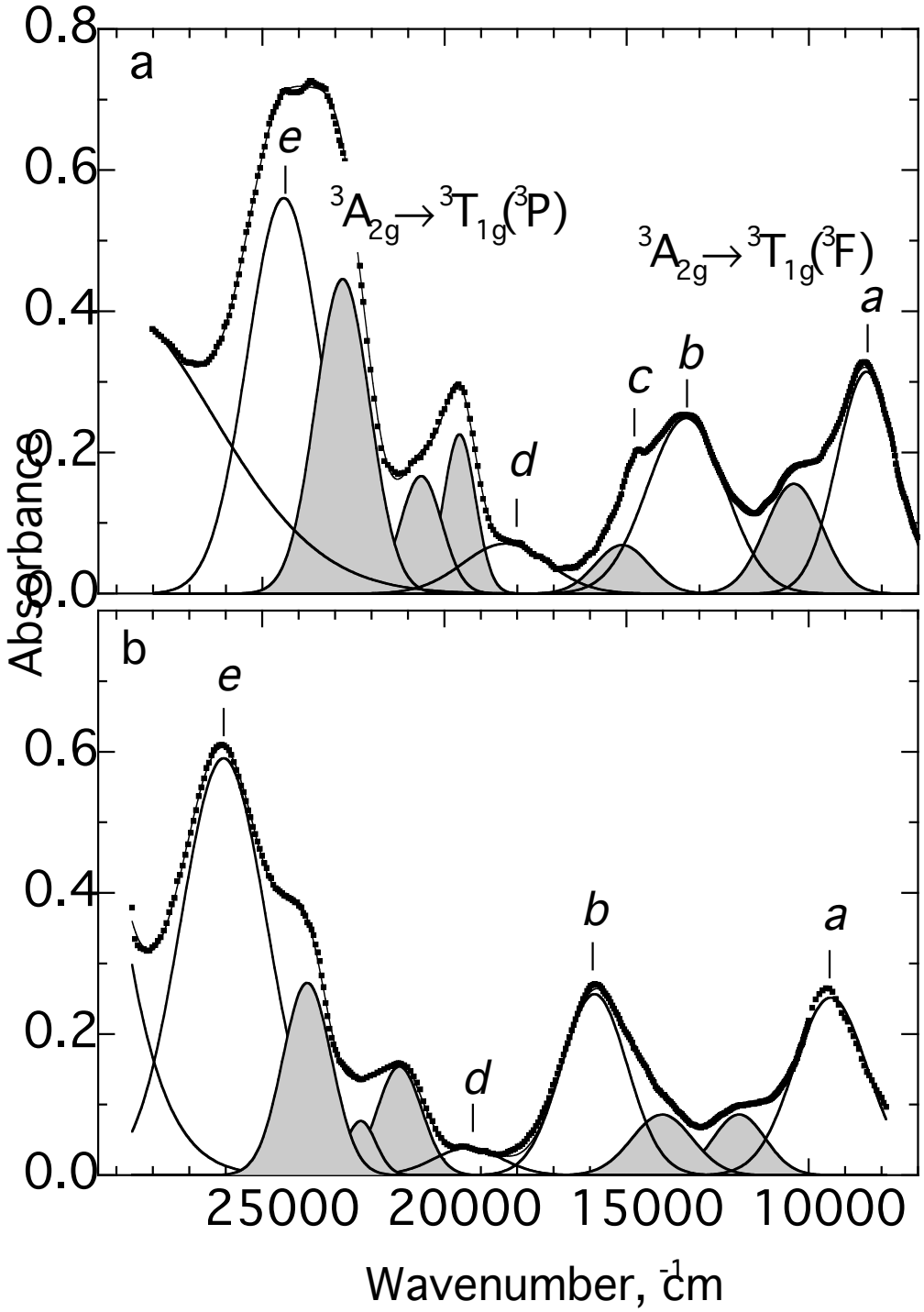

Fig. 7. Curve-resolved spectra of $Ni_{1.0}$ pyroxene measured at two different pressures: **a** –ambient pressure; **b** – 10.48 GPa. Spin-allowed transitions of Ni^{2+}(M1) are designated as *a*-, *b*- and *e*-bands. The bands attributed to the spin-allowed transitions of Ni^{2+}(M2) are shown by the filled Gaussians.